

Structure–Activity Relationships

Surfactant-Assisted Nanocrystalline Zinc Coordination Polymers: Controlled Particle Sizes and Synergistic Effects in Catalysis

Chao Huang, Huarui Wang, Xiaolu Wang, Kuan Gao, Jie Wu,* Hongwei Hou,* and Yaoting Fan^[a]

Abstract: Different morphologies and particle sizes of two crystalline zinc-based coordination polymers (CPs), $[\text{Zn}(\text{pytz})\text{-H}_2\text{O}]_n$ (**1**; $\text{H}_2\text{pytz} = 2,6\text{-bis}(\text{tetrazole})\text{pyridine}$) and $[\text{Zn}_2(\text{pytz})_2\text{4H}_2\text{O}]$ (**2**), from the bulk scale to the nanoscale, could be obtained under solvothermal conditions with different surfactants (polyvinylpyrrolidone (PVP) or polyethylene glycol (PEG) 2000) as templates. PVP and PEG 2000 could act as capping and structure-directing agents, respectively, to influence the growth of crystalline particles and

control their sizes. CP **1** exhibits a two-dimensional framework with window-like units and **2** shows a bimetallic structure. Nanocrystalline **1** and **2** were used as heterogeneous catalysts to study how adjacent catalytic active sites synergistically effected their catalytic reactivities in the direct catalytic conversion of aromatic dinitriles into oxazolines. The results showed that **1** produced bis-oxazolines as the sole products, whereas **2** gave the mono-oxazolines as the major products under the same reaction conditions.

Introduction

Coordination polymers (CPs) made from metal ions linked by organic ligands have provided an interesting platform for engineering immobilizing well-defined molecular catalysts and attracted a growing amount of interest in CP-based heterogeneous catalysis.^[1–4] Compared with homogeneous catalysts and other heterogeneous systems, CP-based heterogeneous catalysts have many advantages, such as a high level of porosity, uniform and accessible catalytic centers, extensive structural and functional variations of the frameworks, and enhanced catalytic activity by eliminating multimolecular catalyst deactivation pathways.^[5–8] To date, various CPs have been explored as catalysts for aldol condensation,^[9,10] C–C bond formation,^[11,12] epoxidations,^[13,14] oxidations,^[15,16] cyclization,^[17,18] and many other reactions.^[7,19,20] Current research hot topics for CP-based catalysts focus mostly on the introduction of catalytically active centers (metal/organic catalyst and privileged catalyst unit) into frameworks with large, accessible pores/channels, which allow facile diffusion of substrates and products, and thus, catalytic conversion along with size, chemo-, and enantioselectivity, depending on the shape and size of the cavities (pores).^[18–22] Additionally, it is desired to tune the morphologies and particle sizes of CPs for their unique size-dependent prop-

erties. For example, bulk-phase CPs are realistically expected to be engineered for a number of bulk-scale applications, including gas storage and nonlinear optics.^[23–27] In contrast, CPs need to be scaled down to the nanoregime to form nanoscale CPs for use as heterogeneous catalysts because they not only maintain structural diversity and physicochemical properties of bulk-phase CPs, but also exhibit particle dimensions in the tens to hundreds of nanometers range, which endows them with higher catalytic efficiency.^[28,29]

Due to their well-defined crystalline nature, another very valuable feature of CPs is that they can provide atomistically well-defined isolated active catalytic sites with uniformly fixed azimuth values and distances throughout the solid to mimic the site isolation of many catalytic enzyme assemblies in nature.^[30,31] These identical/distinct isolated and adjacent active sites can facilitate synergistic interactions with substrates in a sequential or cooperative manner to achieve tandem or cooperative catalytic products without isolation of intermediates; this provides a new economic approach to perform multicomponent reactions.^[32–34] For example, Ma et al. reported the use of postsynthetic modification (PSM) methods to obtain a bifunctional Lewis acid@Brønsted acid heterogeneous catalyst, MIL-101-Cr-SO₃H·Al^{III}, which demonstrated excellent catalytic performance in a series of fixed-bed reactions because of the synergy between the Brønsted acid framework and Lewis acid centers.^[35] However, only a few CPs that take advantage of isolated active sites to achieve multiple activation processes in the catalytic cycle have been prepared by pre-functionalization to combine more than one catalytic site or PSM methods to incorporate additional catalytic moieties in CPs.^[35–46] Exerting precise control over site isolation or adjacent cooperative sites to achieve cooperative or tandem catalytic activities and selectivities is still a considerable challenge.

[a] C. Huang, H. Wang, X. Wang, K. Gao, Prof. J. Wu, Prof. H. Hou, Prof. Y. Fan
The College of Chemistry and Molecular Engineering
Zhengzhou University, Henan 450052 (P.R. China)
E-mail: wujie@zzu.edu.cn
houhongw@zzu.edu.cn

Supporting information and ORCID number from the author for this article are available on the WWW under
<http://dx.doi.org/10.1002/chem.201505009>.

Herein, we report the synthesis of two zinc-based CPs, $[\text{Zn}(\text{pytz})\text{H}_2\text{O}]_n$ (**1**; H_2pytz = 2,6-bis(tetrazole)pyridine) and $[\text{Zn}_2(\text{pytz})_2\text{4H}_2\text{O}]$ (**2**), which are effective heterogeneous catalysts and exhibit different catalytic selectivities for the cyclization reaction of aromatic dinitriles and β -aminoalcohols due to their distinct synergistic effects. In addition, different morphologies and particle sizes of **1** and **2** from the bulk phase to the nanoscale can be obtained with the addition of different surfactants as templates.

Results and Discussion

Design and crystal structures of **1** and **2**

To design and construct N-heterocycle-based zinc(II) CPs as catalysts, we chose a rigid and V-shaped bis-tetrazole ligand, H_2pytz , due to its multiple Lewis base sites with the intention of forming porous CPs with functional groups and the ability to maintain the potential reactivity of the zinc(II) active metal center. In addition, the modular de novo construction of Zn CPs is ideal for the integration of multiple active centers, which may facilitate cooperative catalysis with substrates through multimolecular activation pathways. Thus, the reaction of H_2pytz and Zn^{II} in $\text{H}_2\text{O}/\text{DMF}/\text{MeCN}$ or $\text{H}_2\text{O}/\text{DMF}$ under solvothermal conditions afforded single crystals of **1** or **2** with dimensions of $0.26 \times 0.24 \times 0.21$ or $0.22 \times 0.19 \times 0.18 \text{ mm}^3$, respectively. Single-crystal X-ray crystallography of **1** revealed a 2D microporous framework that exhibited a window-like architecture, in which the windows, square-planar $[\text{Zn}_4(\text{pytz})_2]^{4+}$ units, formed from four Zn^{II} ions in the vertexes with $\text{Zn} \cdots \text{Zn}$ distances of 6.53, 8.69, and 9.68 Å (considering van der Waals radii), respectively (Figure 1a). The two tetrazole rings in the pytz^{2-} ligand are completely deprotonated with dihedral angles between the pyridine and tetrazole rings of 7.62° , and therefore, the rigid, V-shaped ligands adopt a chelate-bridging coordination mode to bridge Zn^{II} ions and form a 2D framework (Figure S1b in the Supporting Information). In comparison, the structure of **2** is distinctly different from that of **1**. In **2**, the pytz^{2-} ligands are nearly coplanar and adopt a bridging coordination mode to connect two Zn^{II} ions, giving a bimetallic structure with $\text{Zn} \cdots \text{Zn}$ distances of 4.28 Å (Figure 1b). Each Zn^{II} center is surrounded by two coordinated water molecules, which are located in the two axial positions of the octahedron. Removing solvent molecules will leave unsaturated coordination positions of catalytically active metal sites free to capture substrates.

Synthesis of difference morphologies and particle sizes of **1** and **2**

Heterogeneous catalysts often display size-dependent physical and chemical properties because the activity depends on the surface area and substrate transport. The advantage of crystalline nanoscale CPs as heterogeneous catalysts is that they exhibit large specific surface areas and hold much promise for a high density of catalytically active sites and unique cooperative effects in liquid-phase heterogeneous catalysis. Therefore,

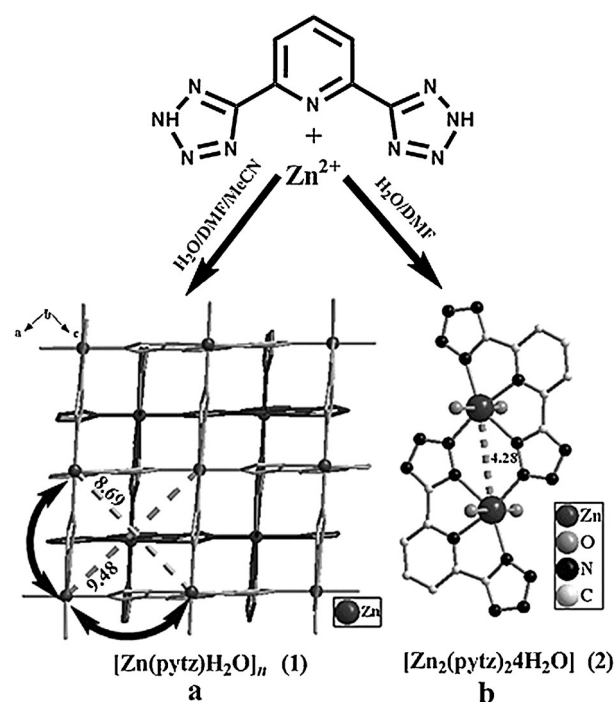


Figure 1. Syntheses of **1** and **2** from the ligand H_2pytz and Zn^{II} . a) View of the stacking 2D window network of **1** and the $\text{Zn} \cdots \text{Zn}$ distances in the window of 6.53, 8.69 and 9.68 Å (considering van der Waals radii). Hydrogen atoms are omitted for clarity. b) View of the bimetallic structure of **2** with $\text{Zn} \cdots \text{Zn}$ distances of 4.28 Å (considering van der Waals radii).

a number of strategies have been developed to control the size and shape of the crystals, including water-in-oil microemulsions, surfactant-mediated hydrothermal syntheses, and high-temperature routes.^[47–50] Herein, with the addition of surfactant (polyvinylpyrrolidone (PVP) or polyethylene glycol (PEG) 2000) as templates, different morphologies and particle sizes of **1** and **2**, from the bulk phase to nanoscale crystals, have been obtained through hydrothermal syntheses. As shown in Figure 2b and e, by employing PVP as a surfactant, the dimensions of **1** and **2** could be scaled down to the nanometer regime of approximately 1.0 μm in length by 500 nm in width for **1** and 500 nm in length by 300 nm in width for **2**. However, with PEG 2000 as a surfactant, the sizes could increase enormously and bulk crystals of **1** and **2** with dimensions of $3.5 \times 3.0 \times 1.5$ and $1.5 \times 1.0 \times 0.7 \text{ mm}^3$, respectively, were produced (Figure 2c and f). The reason for different morphologies and particle sizes of CPs could be attributed to the effect of the surfactants. PVP acted as a capping agent to block the growth of crystalline particles and the growth processes could be quenched at an early stage.^[51] In contrast, PEG 2000 had a structure-directing role, which resulted in an intertwining effect on the crystal surface and facilitated the crystal to undergo a larger growth process.^[52] In addition, powder XRD analysis demonstrated that there was no significant changes between results for simulated and synthesized bulk phase and nanoscale crystals of **1** and **2**, which indicated that the bulk and nanoscale crystals were crystalline and had the same crystal structures (Figure 2g and f).

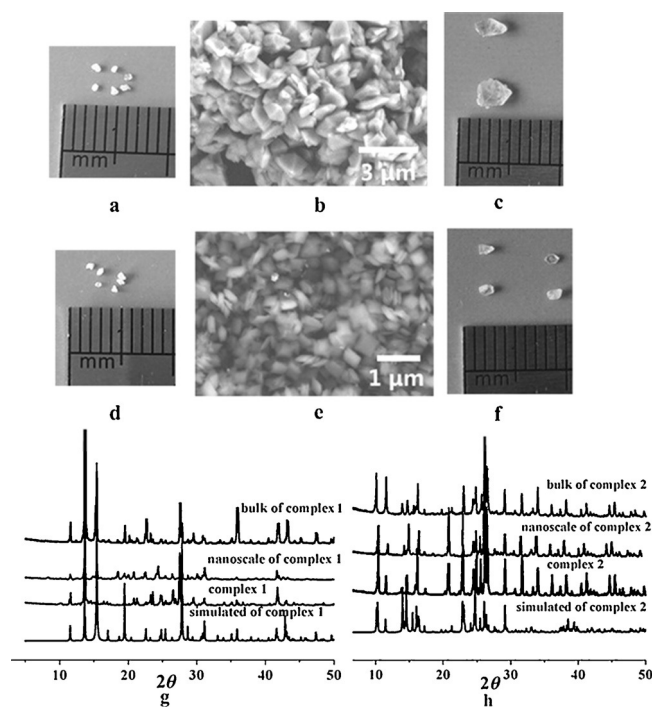


Figure 2. a) The particle sizes of **1**. b) The morphologies and particle sizes of **1** induced by PVP. c) The bulk crystals of **1** induced by PEG 2000. d) The particle sizes of **2**. e) The morphologies and particle sizes of **2** induced by PVP. f) The bulk crystals of **2** induced by PEG 2000. A comparison of the powder XRD results of simulated and synthesized bulk, nanoscale crystals of **1** (g) and **2** (h).

To explore the influence of the concentrations of surfactants upon the formation of particle sizes, numerous attempts at synthesizing crystalline **1** and **2** with different morphologies and particle sizes were made by using different concentrations of PVP and PEG 2000 (0.2, 0.15, 0.10, 0.05, and 0.02 g). The results indicated that when the concentrations of PVP and PEG 2000 were 0.05 and 0.2 g, respectively, well-defined morphologies and particle size distributions of **1** and **2** could be produced. This might be attributed to PVP and PEG 2000, which could alter the relative kinetics of nucleation and crystal growth in support of the formation of well-defined morphologies and particle sizes.

In addition, other methods, such as water-in-oil, microemulsion, and high-temperature routes, always led to the formation of amorphous CPs rather than crystalline CPs. Therefore, this work illustrates the ability to tune the size of CPs with the same framework from the bulk scale to the nanoscale by exploiting different surfactants as templates.

Catalytic effects of **1** and **2**

For the cyclization of aromatic dinitriles and β -aminoalcohols, it remains a synthetic challenge to develop strategies to selectively achieve mono- or bis-oxazolines, which are used directly to synthesize some natural products and are useful ligands in asymmetric reactions, according to the requirements of green chemistry. However, exploration of this reaction under a variety

of catalytic conditions (e.g., diisopropylcarbodiimide (DIC), silica sulfuric acid (SSA), InCl_3 , ZnCl_2 , FeCl_3) usually afforded a mixture of bis- and mono-oxazolines under harsh reaction conditions (strong acidic, toxic solvents, complex reagents, etc.)^[53–58] Inspired by the merits of CP-based catalysts with synergistic effects, we were interested in exploring whether CPs as heterogeneous solid catalysts could achieve high catalytic selectivity for the reactions to yield mono- or bis-oxazolines as a result of mono- or bimolecular activation pathways, respectively.

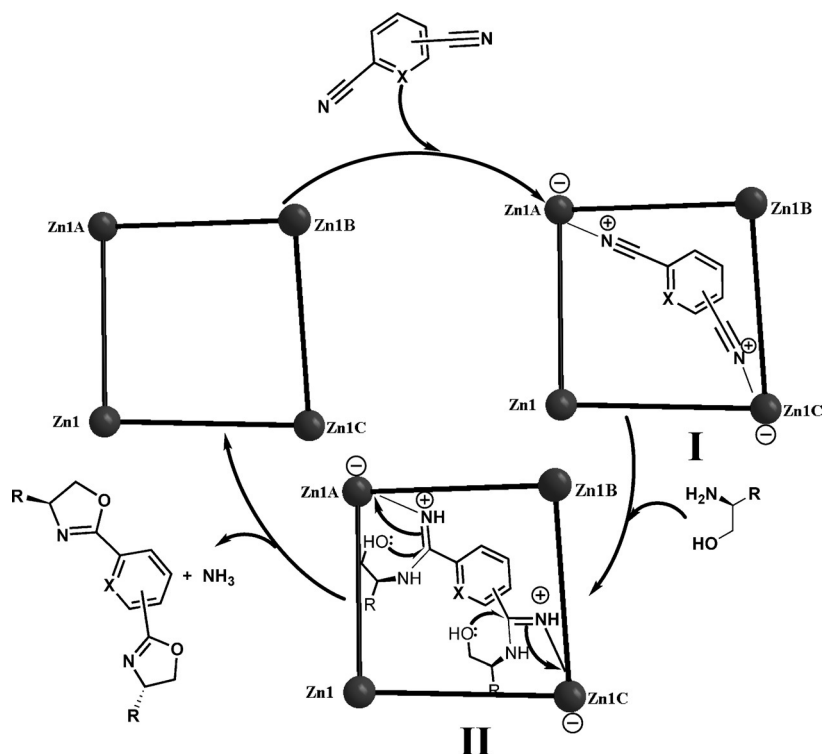
With the treatment of (*S*)-valinol (**3**) or *D*-2-phenylglycinol (**4**) with aromatic dinitriles (Ar = phenyl, pyridyl; **5a–e**) in the presence of nanoscale **1** or **2** as heterogeneous catalysts at reflux for 15 h, the cyclization reaction proceeded successfully and provided the products in good yields (Table 1). In all cases, heterogeneous catalyst **1** produced bis-oxazolines as the sole products with yields ranging from 84 to 91% (**6a–d** and **7a–d**), whereas heterogeneous catalyst **2** gave mono-oxazolines as the major products with yields ranging from 79 to 89% (**8a–e** and **9a–e**), along with a small amount of bis-oxazoline products (<8%). In comparison, the homogeneous catalyst ZnCl_2 , a commonly used Lewis acid catalyst for the cyclization of aromatic dinitriles and β -aminoalcohols, gave both the mono- and bis-oxazoline cyclization products under the same reaction conditions (Table 1). Only under more harsh conditions, such as water-free, oxygen-free, and high pressure, could bis-oxazolines be obtained as the sole products with yields ranging from 51 to 61% in 72 h.^[58]

The distinct and high regioselectivity of the catalytic reaction indicates that the reactions catalyzed by CPs **1** and **2** might go through a different pathway. Because the catalytic active sites in the CPs are positioned in the frameworks periodically with identical distances between nearest neighbors, they may synergistically influence the catalytic reactivities to produce tandem or cooperative catalytic products. A single-crystal structural study indicates that the structure of **1** contains the window-like framework; the corners of the windows are occupied by four Zn^{II} ions at distances of 6.53, 8.69, and 9.68 Å. In addition, the window surface is occupied by coordinated water molecules, which are good leaving groups and will be good for making contacts between organic substrates and the catalytic active sites in the reaction process. By comparing the $\text{Zn}\cdots\text{Zn}$ distances and dimensions of substrates **5a–d** (Table 1), we deduced that the Zn^{II} centers in **1** could simultaneously activate the two cyano groups of aromatic dinitriles **5a–d** (Figure S3 in the Supporting Information). In contrast, because the dimensions of 1,1'-biphenyl-4,4'-dicarbonitrile (**5e**) did not fit in the $\text{Zn}\cdots\text{Zn}$ distances of **1**, only the mono-oxazoline cyclization products (**8e** and **9e**) were obtained. Thus, we hypothesized that the four zinc centers on the surface of the windows could stabilize the aromatic dinitriles, provide a platform to perform reactions in the windows, and display synergistic effects and shape-selective catalytic capabilities. As a consequence, a plausible catalytic cycle is proposed (Scheme 1). The dinitrile groups were first activated by Zn^{II} centers in the windows to form dinitrile cations **I**. Subsequently, β -aminoalcohols attacked **I** to afford the intermediate products **II**. Finally, the

Table 1. Nanoscale of 1 and 2 Catalyzed aromatic dinitriles to bis/mono-oxazolines.^[a]

Entry	Catalyst	5	Yield [%]			
			6 a-e ^[b]	7 a-e ^[b]	8 a-e ^[b]	9 a-e ^[b]
<p> $\text{R-CH(OH)-CH}_2\text{-NH}_2$ (3.0 mmol) + $\text{NC-C}_6\text{H}_3\text{(X)-CN}$ (1.0 mmol) </p> <p> 1 (0.1 mmol) → chlorobenzene, reflux → 6a-d (R = <i>i</i>Pr), 7a-d (R = Ph) </p> <p> 2 (0.1 mmol) → chlorobenzene, reflux → 8a-e (R = <i>i</i>Pr), 9a-e (R = Ph) </p> <p> 5a = 4-NCC₆H₄ 5b = 3-NCC₆H₄ 5c = 6-NCC₆H₃N 5d = 2-NCC₆H₄ 5e = 4-NCC₁₃H₈ </p>						
1	1	8.00 Å	91	89	–	–
2	2	<p>5a 8.00 Å 4.30 Å</p>	–	–	89	86
3	ZnCl ₂		43	48	56	51
4	1		6.94 Å	89	88	–
5	2	<p>5b 6.94 Å 4.96 Å</p>	–	–	87	84
6	ZnCl ₂		41	45	55	56
7	1		6.74 Å	86	86	–
8	2	<p>5c 6.74 Å 4.55 Å</p>	–	–	85	84
9	ZnCl ₂		51	49	46	48
10	1		5.52 Å	84	84	–
11	2	<p>5d 5.52 Å 4.96 Å</p>	–	–	82	82
12	ZnCl ₂		46	44	53	52
13	1		12.49 Å	–	–	81
14	2	<p>5e 12.49 Å 4.30 Å</p>	–	–	79	78
15	ZnCl ₂		41	40	39	38

[a] Reaction conditions: β -aminoalcohols (3.0 mmol), aromatic dinitriles (1.0 mmol), catalyst (0.1 mmol), chlorobenzene (5 mL), 15 h. [b] Yield of product isolated after 15 h.



Scheme 1. Proposed mechanism for the synthesis of bis-oxazolines catalyzed by synergistic effects on the surface of zinc-based CP 1.

corresponding bis-oxazolines were produced by releasing NH_3 and the catalyst for the next catalytic cycle.

In contrast, the Zn...Zn distance of the binuclear Zn centers in **2** is 4.28 Å, which is too short to cooperatively activate both cyano groups of **5a–e**. In this case, the binuclear zinc ions could not afford the equivalent active centers to ensure that the two cyano groups of aromatic dinitriles were simultaneously activated in the cyclization reaction.

To prove that activation of the cyclization species occurred on the surface rather than in the pores of the solid catalyst, the cyclization of **3** and **5a** was carried out with bulk crystals of **1** ($\approx 3.5 \times 3.0 \times 1.5 \text{ mm}^3$) under the same reaction conditions. Less than 18% yield was observed after 15 h, which was much lower than the 91% yield obtained with crystalline nanoscale **1**. Furthermore, 44% yield was obtained by using large crystals ($\approx 0.26 \times 0.24 \times 0.21 \text{ mm}^3$) of **1** after 15 h; this clearly demonstrated that the catalytic activities relied on the surface catalytic sites of particle sizes. The different yields obtained with nanoscale and bulk crystals could be attributed to the experimentally determined BET surface area. Nitrogen sorption measurements after supercritical (SC) CO_2 activation showed that the experimentally determined BET surface areas were 9.2516 and $0.5358 \text{ m}^2 \text{ g}^{-1}$ for nanoscale and bulk crystals, respectively. In further studies, due to low N_2 uptake, the pore size distributions (PSDs) of **1** afforded a narrow range. In addition, PLATON analysis gave no free void volume ratio in **1**, which suggested that **1** was completely nonporous. Therefore, these results provided evidence that the catalytic reactions took place on the surface of the CP crystals with synergistic effects rather than in the interior of the crystals.

The leaching of zinc from the crystals of **1** and **2** during the reaction was examined by atomic absorption spectroscopy (AAS) analysis, and only slight leaching ($< 1 \text{ ppm}$) was observed. Next, we carried out a filtration experiment. After 25 or 21% conversion of **5a** in the presence of **1** or **2** in 1 h, the reaction mixture was passed through a sand core funnel to remove the catalyst, and the supernatant was allowed to stand for 14 h. It was found that the conversion of the supernatant remained almost unchanged during this time. Thus, these experiments unambiguously demonstrated that **1** and **2** were truly heterogeneous catalysts.

To evaluate the stability of the solid catalysts, we also examined recycled and reused **1** and **2** for this catalytic reaction with **5a**. Upon completion of the reaction, the catalysts could be readily recovered from the catalytic reaction by centrifugation and the recovered catalysts showed only slight deterioration after five runs. Moreover, the powder XRD patterns of these **1** and **2** crystallites after the fifth catalytic reaction closely matched those of single crystals of **1** and **2**, and showed no signs of framework collapse and decomposition, which indicated that the framework could remain intact after at least five runs (Figure 3).

Conclusion

We demonstrated a rare example of regulating different morphologies and particle sizes of Zn CPs from the bulk phase to the nanoscale by using different surfactants. PVP could scale down the dimensions of the CPs to the nanometer regime, whereas PEG 2000 favored the formation of the bulk phase

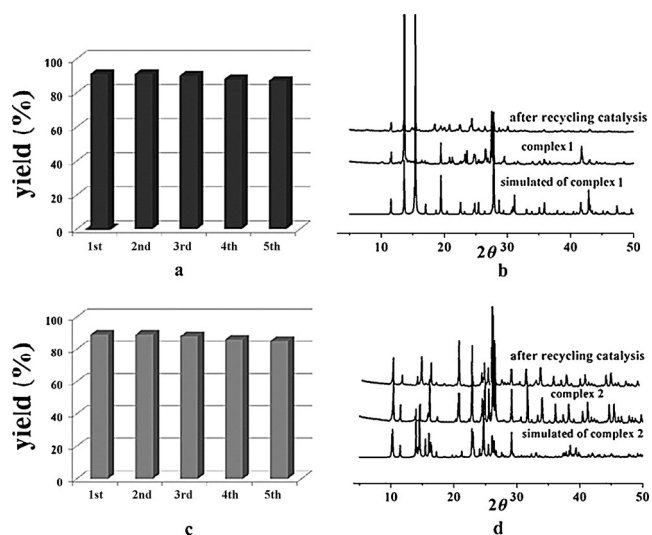


Figure 3. a) Recycling test for the conversion of aromatic dinitriles into bis-oxazolines with nanoscale **1**. b) A comparison of the powder XRD patterns of **1** before and after catalysis. c) Recycling test for the conversion of aromatic dinitriles into mono-oxazolines with nanoscale **2**. d) A comparison of the powder XRD patterns of **2** before and after catalysis.

under the same reaction conditions. For the cyclization reaction of aromatic dinitriles and β -aminoalcohols, CPs **1** and **2** could achieve high catalytic selectivity to yield bis- or mono-oxazolines as a result of bi- or unimolecular activation pathways, respectively. The four Zn^{II} centers in **1** could follow cooperative bimetallic catalysis in which the two cyano groups of the aromatic dinitriles were activated simultaneously. Nevertheless, the Zn^{II} centers in **2** were shown to be independently catalytically active as a result of unimolecular activation pathways. We also showed that the CPs maintained their crystallinity after the catalytic reaction. This work illustrated the ability to synthesize CPs with different sizes from the bulk scale to the nanoscale and provided important insights into CP-catalyzed cooperative reactions.

Experimental Section

Materials and physical measurements

All reagents and solvents were commercially available and used as received without further purification. FTIR spectra were recorded on a Bruker-ALPHA spectrophotometer as KBr pellets in the $\tilde{\nu}$ = 400–4000 cm⁻¹ region. Elemental analyses (C and H) were carried out on a FLASH EA 1112 elemental analyzer. Powder XRD patterns were recorded by using Cu_{K α} 1 radiation on a PANalyticalX'Pert PRO diffractometer. A Hitachi TM-1000 field-emission scanning electron microscope was used to image the particle sizes and morphologies. Thermal analyses were performed on a Netzsch STA 449C thermal analyzer at a heating rate of 10 °C min⁻¹ in air. ¹H and ¹³C NMR spectra were obtained on a Bruker Avance-400 spectrometer. HRMS-ESI was performed on a MicroTM Q-TOF mass spectrometer. AAS was performed on a Z28000 graphite-oven atomic absorption spectrophotometer. The PSDs of **1** were collected on a Micromeritics ASAP 2420 accelerated surface area and porosimetry system under ultrahigh vacuum in a clean system, with a diaphragm and turbo pumping system. Ultrahigh-purity grade (>

99.999%) N₂ gas was applied in all adsorption measurements. The experimental temperature was maintained by using liquid nitrogen (77 K). Prior to measurements, bulk samples of **1** and **2** were washed with absolute ethanol three times, dried under vacuum, and then transferred onto a stainless-steel column. After 20 min of soaking and venting of SC-CO₂ by means of a DB-80 simplex pump, the column pressure regulator was set at 109 bar by soaking with SC-CO₂, and the column temperature was raised to 60 °C. SC-CO₂ in the column was gradually vented after 12 h.

Synthesis of **1**

A mixture of ZnSO₄·7H₂O (0.20 g, 0.70 mmol), H₂pytz (0.10 g, 0.47 mmol), H₂O (2 mL), CH₃CN (5 mL), and DMF (3 mL) was placed in a 25 mL Teflon-lined stainless-steel container. The mixture was sealed and heated at 120 °C for 3 days. After the mixture was cooled to ambient temperature at a rate of 5 °C h⁻¹, colorless crystals of **1** were obtained (82%, based on Zn). IR (KBr): $\tilde{\nu}$ = 3357 (m), 3086 (m), 2168 (w), 2042 (vw), 1620 (s), 1585 (s), 1435 (vs), 1185 (vs), 1087 (s), 835 (vs), 794 (s), 759 (w), 738 cm⁻¹ (w); elemental analysis calcd (%) for C₇H₅ZnN₉O: C 28.35, H 1.70, N 42.50; found: C 28.37, H 1.67, N 42.47.

Synthesis of bulk crystals of **1** with PEG 2000

A solution of ZnSO₄·7H₂O (0.10 g, 0.35 mmol) and PEG 2000 (0.20 g) in water (2 mL) was sonicated for 10 min. A mixture of CH₃CN (5 mL), DMF (3 mL), and H₂pytz (0.05 g, 0.24 mmol) was added to the mixture in PEG/H₂O and sonicated for another 20 min. Subsequently, the solution was transferred to a 25 mL Teflon-lined stainless-steel container to allow crystal growth at 120 °C for 3 days. After the mixture was cooled to ambient temperature at a rate of 5 °C h⁻¹, colorless bulk crystals of **1** were obtained.

Synthesis of nanocrystals of **1** with PVP

A mixture of ZnSO₄·7H₂O (0.40 g, 1.40 mmol), PVP (0.050 g), and H₂O (2 mL) was sonicated for 20 min until all PVP was dissolved. A solution of CH₃CN (5 mL), DMF (3 mL), and H₂pytz (0.20 g, 0.94 mmol) was added to the mixture in PVP/H₂O and sonicated for another 20 min. Subsequently, the solution was transferred to a 25 mL Teflon-lined stainless-steel container to allow crystal growth at 120 °C for 3 days. After cooling, the nanocrystals were isolated by centrifugation at 10000 rpm for 10 min. After removal of the supernatant, the nanocrystals were washed by sonication after being redispersed in EtOH (5 mL). The suspension in EtOH was then centrifuged again for 10 min at 10000 rpm to recover the nanocrystals.

Synthesis of **2**

A mixture of Zn(NO₃)₂·6H₂O (0.059 g, 0.20 mmol), H₂pytz (0.022 g, 0.1 mmol), H₂O (5 mL), and DMF (3 mL) was placed in a 25 mL Teflon-lined stainless-steel container. The mixture was sealed and heated at 120 °C for 3 days. After the mixture was cooled to ambient temperature at a rate of 5 °C h⁻¹, colorless crystals of **2** were obtained (82%, based on Zn). IR (KBr): $\tilde{\nu}$ = 3593 (m), 3409 (m), 3091 (m), 2168 (w), 2049 (vw), 1617 (s), 1580 (m), 1436 (vs), 1178 (s), 1048 (vw), 827 (s), 789 (s), 757 (s), 663 cm⁻¹ (m); elemental analysis calcd (%) for C₁₄H₁₄Zn₂N₁₈O₄: C 26.72, H 2.42, N 40.07; found: C 26.75, H 2.39, N 40.06.

Synthesis of bulk crystals of **2** with PEG 2000

A solution of $\text{Zn}(\text{NO}_3)_2 \cdot 6\text{H}_2\text{O}$ (0.118 g, 0.40 mmol) and PEG 2000 (0.20 g) in water (5 mL) was sonicated for 10 min. A mixture of DMF (3 mL) and H_2pytz (0.043 g, 0.2 mmol) was added to the mixture of PEG/ H_2O and sonicated for another 20 min. Subsequently, the solution was transferred to a 25 mL Teflon-lined stainless-steel container to allow crystal growth at 120°C for 3 days. After the mixture was cooled to ambient temperature at a rate of 5°C h^{-1} , colorless bulk crystals of **2** were obtained.

Synthesis of nanocrystals **2** with PVP

A mixture of $\text{Zn}(\text{NO}_3)_2 \cdot 6\text{H}_2\text{O}$ (0.118 g, 0.40 mmol), PVP (0.050 g), and H_2O (5 mL) was sonicated for 20 min until all PVP was dissolved. A solution of DMF (3 mL) and H_2pytz (0.043 g, 0.20 mmol) was added to the mixture of PVP/ H_2O and sonicated for another 20 min. Subsequently, the solution was transferred to a 25 mL Teflon-lined stainless-steel container to allow crystal growth at 120°C for 3 days. After cooling, the nanocrystals were isolated by centrifugation at 10000 rpm for 10 min. After removal of the supernatant, the nanocrystals were washed by sonication after being redispersed in EtOH (5 mL). The suspension in EtOH was then centrifuged again for 10 min at 10000 rpm to recover the nanocrystals.

Typical procedure for a tandem condensation–cyclodehydration reaction for the synthesis of oxazoline

Nanoscale Zn^{II} complex (0.1 mmol, 0.1 equiv based on zinc ions) was added to a solution of chlorobenzene (5 mL) charged with β -aminoalcohols (3.0 mmol) and aromatic dinitriles (1.0 mmol). The resulting mixture was heated at reflux and monitored by TLC. After completion of the reaction (approximately 15 h), the mixture was cooled to room temperature, and diluted with ethyl acetate. The product was then centrifuged and extracted with brine (3×10 mL). The organic phases were combined, dried over anhydrous Na_2SO_4 , and concentrated under reduced pressure. The residue was purified by column chromatography on silica gel to give the pure product.

Crystal data collection and refinement

The data for **1** and **2** were collected on a Rigaku Saturn 724 CCD diffractometer ($M_o_{K\alpha}$, $\lambda = 0.71073 \text{ \AA}$) at $(20 \pm 1)^\circ\text{C}$. Absorption corrections were applied by using a numerical program. The data were corrected for Lorentz and polarization effects. The structures were solved by direct methods and refined by a full-matrix least-squares technique based on F^2 with the SHELXL-97 crystallographic software package.^[59] The hydrogen atoms were placed at calculated positions and refined as riding atoms with isotropic displacement parameters. Crystallographic crystal data and structure processing parameters for **1**, **2**, and parts of complexes under specific conditions are summarized in Table S1 in the Supporting Information. Selected bond lengths and angles for **1**, **2**, and parts of complexes under specific conditions are listed in Table S2 in the Supporting Information.

CCDC 1414110 (**1**) and 1414111 (**2**) contain the supplementary crystallographic data for this paper. These data are provided free of charge by The Cambridge Crystallographic Data Centre.

Acknowledgements

This work was financially supported by the National Natural Science Foundation of China (nos. 21201152 and 21371155) and the Research Fund for the Doctoral Program of Higher Education of China (20124101110002).

Keywords: cooperative effects • coordination polymers • heterogeneous catalysts • nanostructures • structure–activity relationships

- [1] J. M. Falkowski, S. Liu, W. Lin, *Isr. J. Chem.* **2012**, *52*, 591–603.
- [2] C. Wang, M. Zheng, W. Lin, *J. Phys. Chem. Lett.* **2011**, *2*, 1701–1709.
- [3] L. Ma, J. M. Falowski, C. Abney, W. Lin, *Nat. Chem.* **2010**, *2*, 838–846.
- [4] A. H. Chughtai, N. Ahmad, H. A. Younus, A. Laypkov, F. Verpoort, *Chem. Soc. Rev.* **2015**, *44*, 6804–6849.
- [5] L. Ma, C. Abney, W. Lin, *Chem. Soc. Rev.* **2009**, *38*, 1248–1256.
- [6] M. Yoon, R. Srirambalaji, K. Kim, *Chem. Rev.* **2012**, *112*, 1196–1231.
- [7] J. Lee, O. K. Farha, J. Roberts, K. A. Scheidt, S. T. Nguyen, J. T. Hupp, *Chem. Soc. Rev.* **2009**, *38*, 1450–1459.
- [8] A. Dhakshinamoorthy, M. Alvaro, H. Garcia, *Chem. Commun.* **2010**, *46*, 6476–6478.
- [9] A. Dhakshinamoorthy, M. Alvaro, P. Horcajada, E. Gibson, M. Vishnuvarthan, A. Vimont, J. Grenèche, C. Serre, M. Daturi, H. Garcia, *ACS Catal.* **2012**, *2*, 2060–2065.
- [10] S. Horike, M. Dincă, K. Tamaki, J. R. Long, *J. Am. Chem. Soc.* **2008**, *130*, 5854–5855.
- [11] J. M. Roberts, B. M. Fini, A. A. Sarjeant, O. K. Farha, J. T. Hupp, K. A. Scheidt, *J. Am. Chem. Soc.* **2012**, *134*, 3334–3337.
- [12] F. Song, C. Wang, J. M. Falkowski, L. Ma, W. Lin, *J. Am. Chem. Soc.* **2010**, *132*, 15390–15398.
- [13] S. Cho, B. Ma, S. T. Nguyen, J. T. Hupp, T. E. Albrecht-Schmitt, *Chem. Commun.* **2006**, 2563–2565.
- [14] F. Carson, S. Agrawal, M. Gustafsson, A. Bartoszewicz, F. Moraga, X. Zou, B. Martín-Matute, *Chem. Eur. J.* **2012**, *18*, 15337–15344.
- [15] L. Ma, X. Wang, D. Deng, F. Luo, B. Ji, J. Zhang, *J. Mater. Chem. A* **2015**, *3*, 20210–20211.
- [16] C. Huang, R. Ding, C. Song, J. Lu, L. Liu, X. Han, J. Wu, H. Hou, Y. Fan, *Chem. Eur. J.* **2014**, *20*, 16156–16163.
- [17] R. Ding, C. Huang, J. Lu, J. Wang, C. Song, J. Wu, H. Hou, Y. Fan, *Inorg. Chem.* **2015**, *54*, 1405–1413.
- [18] J. Zhang, L. Wojtas, R. W. Larsen, M. Eddaoudi, M. J. Zaworotko, *J. Am. Chem. Soc.* **2009**, *131*, 17040–17041.
- [19] D. Farrusseng, S. Aguado, C. Pinel, *Angew. Chem. Int. Ed.* **2009**, *48*, 7502–7513; *Angew. Chem.* **2009**, *121*, 7638–7649.
- [20] P. V. Kortunov, L. Heinke, M. Arnold, Y. Nedellec, D. J. Jones, J. Caro, J. Kärger, *J. Am. Chem. Soc.* **2007**, *129*, 8041–8047.
- [21] J. M. Falkowski, C. Wang, S. Liu, W. Lin, *Angew. Chem. Int. Ed.* **2011**, *50*, 8674–8678; *Angew. Chem.* **2011**, *123*, 8833–8837.
- [22] C. Huang, J. Wu, C. Song, R. Ding, Y. Qiao, H. Hou, J. Chang, Y. Fan, *Chem. Commun.* **2015**, *51*, 10353–10356.
- [23] M. Du, C. Li, M. Chen, Z. Ge, X. Wang, L. Wang, C. Liu, *J. Am. Chem. Soc.* **2014**, *136*, 10906–10909.
- [24] D. Yu, D. Sun, M. Avdeev, X. Tian, Q. Gu, X. Tao, *Cryst. Growth Des.* **2015**, *15*, 3110–3113.
- [25] S. S. Park, E. R. Hontz, L. Sun, C. H. Hendon, A. Walsh, T. V. Voorhis, M. Dincă, *J. Am. Chem. Soc.* **2015**, *137*, 1774–1777.
- [26] F. Wang, F. Li, M. Xu, H. Yu, J. Zhang, H. Xia, J. Lang, *J. Mater. Chem. A* **2015**, *3*, 5908–5916.
- [27] H. Li, Y. Han, Y. Lin, Z. Guo, G. Jin, *J. Am. Chem. Soc.* **2014**, *136*, 2982–2985.
- [28] A. Aijaz, Q. Xu, *J. Phys. Chem. Lett.* **2014**, *5*, 1400–1411.
- [29] M. C. Das, S. Xiang, Z. Zhang, B. Chen, *Angew. Chem. Int. Ed.* **2011**, *50*, 10510–10520; *Angew. Chem.* **2011**, *123*, 10696–10707.
- [30] Y. Chen, V. Lykourinou, C. Vetromile, T. Hoang, L. Ming, R. W. Larsen, S. Ma, *J. Am. Chem. Soc.* **2012**, *134*, 13188–13191.

- [31] Y. Chen, S. Han, X. Li, Z. Zhang, S. Ma, *Inorg. Chem.* **2014**, *53*, 10006–10008.
- [32] T. Zhang, F. Song, W. Lin, *Chem. Commun.* **2012**, *48*, 8766–8768.
- [33] C. Zhu, G. Yuan, X. Chen, Z. Yang, Y. Cui, *J. Am. Chem. Soc.* **2012**, *134*, 8058–8061.
- [34] L. Ma, C. Wu, M. M. Wanderley, W. Lin, *Angew. Chem. Int. Ed.* **2010**, *49*, 8244–8248; *Angew. Chem.* **2010**, *122*, 8420–8424.
- [35] B. Li, K. Leng, Y. Zhang, J. J. Dynes, J. Wang, Y. Hu, D. Ma, Z. Shi, L. Zhu, D. Zhang, Y. Sun, M. Chrzanowski, S. Ma, *J. Am. Chem. Soc.* **2015**, *137*, 4243–4248.
- [36] P. V. Dau, S. M. Cohen, *Inorg. Chem.* **2015**, *54*, 3134–3138.
- [37] J. Song, Z. Luo, D. K. Britt, H. Furukawa, O. M. Yaghi, K. I. Hardcastle, C. L. Hill, *J. Am. Chem. Soc.* **2011**, *133*, 16839–16846.
- [38] Y. Mao, J. Li, W. Cao, Y. Ying, P. Hu, Y. Liu, L. Sun, H. Wang, C. Jin, X. Peng, *Nat. Commun.* **2014**, *5*, 5532.
- [39] J. Li, S. Li, Y. Tang, K. Li, L. Zhou, N. Kong, Y. Lan, J. Bao, Z. Dai, *Sci. Rep.* **2014**, *4*, 5130.
- [40] J. Li, Y. Chen, Y. Tang, S. Li, H. Dong, K. Li, M. Han, Y. Lan, J. Bao, Z. Dai, *J. Mater. Chem. A* **2014**, *2*, 6316–6319.
- [41] Y. Chen, Q. Xu, S. Yu, H. Jiang, *Small* **2015**, *11*, 71–76.
- [42] H. Fei, S. M. Cohen, *J. Am. Chem. Soc.* **2015**, *137*, 2191–2194.
- [43] X. Gu, Z. Lu, H. Jiang, T. Akita, Q. Xu, *J. Am. Chem. Soc.* **2011**, *133*, 11822–11825.
- [44] S. Wang, L. Bromberg, H. Schreuder-Gibson, T. A. Hatton, *ACS Appl. Mater. Interfaces* **2013**, *5*, 1269–1278.
- [45] F. Shieh, S. Wang, C. Yen, C. Wu, S. Dutta, L. Chou, J. V. Morabito, P. Hu, M. Hsu, K. C. W. Wu, C. Tsung, *J. Am. Chem. Soc.* **2015**, *137*, 4276–4279.
- [46] Z. Zhang, Y. Chen, S. He, J. Zhang, X. Xu, Y. Yang, F. Nosheen, F. Saleem, W. He, X. Wang, *Angew. Chem. Int. Ed.* **2014**, *53*, 12517–12521; *Angew. Chem.* **2014**, *126*, 12725–12729.
- [47] M. Oh, C. A. Mirkin, *Nature* **2005**, *438*, 651–654.
- [48] J. Della Rocca, D. Liu, W. Lin, *Acc. Chem. Res.* **2011**, *44*, 957–968.
- [49] R. A. Davidson, T. Guo, *J. Phys. Chem. A* **2014**, *118*, 30221–30228.
- [50] H. Xu, B. W. Zeiger, K. S. Suslick, *Chem. Soc. Rev.* **2013**, *42*, 2555–2567.
- [51] X. Wang, X. Wu, Y. Guo, Y. Zhong, X. Cao, Y. Ma, J. Yao, *Adv. Funct. Mater.* **2010**, *20*, 1680–1686.
- [52] Y. Cui, L. Lei, B. Li, X. Zhou, N. Xu, *J. Phys. Chem. A* **2010**, *114*, 2434–2439.
- [53] H. C. Aspinall, O. Beckingham, M. D. Farrar, N. Greeves, C. D. Thomas, *Tetrahedron Lett.* **2011**, *52*, 5120–5123.
- [54] I. Mohammadpoor-Baltork, V. Mirkhani, M. Moghadam, S. Tangestaninejad, M. A. Zolffiol, M. Abdollahi-Alibeik, A. R. Khosropour, H. Kargar, S. F. Hojati, *Catal. Commun.* **2008**, *9*, 894–901.
- [55] R. Rasappan, D. Laventine, O. Reiser, *Coord. Chem. Rev.* **2008**, *252*, 702–714.
- [56] T. Ohshima, T. Iwaski, K. Mashima, *Chem. Commun.* **2006**, 2711–2713.
- [57] M. Moghadam, V. Mirkhani, S. Tangestaninejad, I. Mohammadpoor-Baltork, H. Kargar, *J. Iraqi Chem. Soc.* **2009**, *6*, 251–258.
- [58] M. Luo, J. H. Zhang, J. Sun, S. M. Zhou, H. Yin, K. L. Hu, *J. Comb. Chem.* **2009**, *11*, 220–227.
- [59] G. M. Sheldrick, *SHELXS97*, Program for the Refinement of Crystal Structures; University of Göttingen, Germany, **1997**.

Received: December 12, 2015

Published online on March 21, 2016